HAL
open science

Area selective deposition of TiO 2 by intercalation of plasma etching cycles in PEALD process: A bottom up approach for the simplification of 3D integration scheme

Rémi Vallat, Rémy Gassilloud, Olivier Salicio, Khalil El Hajjam, Gabriel Molas, Bernard Pelissier, Christophe Vallée

To cite this version:

Rémi Vallat, Rémy Gassilloud, Olivier Salicio, Khalil El Hajjam, Gabriel Molas, et al.. Area selective deposition of TiO 2 by intercalation of plasma etching cycles in PEALD process: A bottom up approach for the simplification of 3D integration scheme. Journal of Vacuum Science & Technology A, 2019, 37 (2), pp.020918. 10.1116/1.5049361 . hal-02108939

HAL Id: hal-02108939

https://hal.univ-grenoble-alpes.fr/hal-02108939

Submitted on 28 Sep 2022

HAL is a multi-disciplinary open access archive for the deposit and dissemination of scientific research documents, whether they are published or not. The documents may come from teaching and research institutions in France or abroad, or from public or private research centers.

L'archive ouverte pluridisciplinaire **HAL**, est destinée au dépôt et à la diffusion de documents scientifiques de niveau recherche, publiés ou non, émanant des établissements d'enseignement et de recherche français ou étrangers, des laboratoires publics ou privés.

Area selective deposition of TiO_2 by intercalation of plasma etching cycles in PEALD process: A bottom up approach for the simplification of 3D integration scheme

Rémi Vallat,[1,2] Rémy Gassilloud,[2] Olivier Salicio,[1] Khalil El Hajjam,[2] Gabriel Molas,[2] Bernard Pelissier,[1] and Christophe Vallée[1,3,a)]
[1]*University of Grenoble Alpes, LTM, F-38000 Grenoble, France*
[2]*CEA, LETI, Minatec Campus, F-38054 Grenoble, France*
[3]*Faculty of Pure and Applied Sciences, University of Tsukuba, Tsukuba 305-8573, Japan*

(Received 20 July 2018; accepted 17 January 2019; published 4 February 2019)

A selective deposition process for bottom-up approach was developed in a modified plasma enhanced atomic layer deposition (PEALD) sequence. As a case study, a very standard PEALD TiO_2 using organo-amine precursor and O_2 plasma is chosen. The metal oxide selectivity is obtained on TiN versus Si-based surfaces by adding one etching/passivation plasma step of fluorine every n cycles in a PEALD-TiO_2 process. Fluorine gas NF_3 allows (1) to etch the TiO_2 layer on Si, SiO_2, or SiN surface while keeping few nanometers of TiO_2 on the TiN substrate and (2) to increase the incubation time on the Si-based surface. *Quasi-in situ* XPS measurements were used to study the incubation time between Si/SiO_2 substrates versus TiN substrate. Results show that Si–F bonds are formed on Si and lock the surface reactions. The effectiveness of this atomic layer selective deposition method was successfully tested on a 3D patterned substrate with the metal oxide deposited only at the edge of metal lines. *Published by the AVS.* https://doi.org/10.1116/1.5049361

I. INTRODUCTION

The present work deals with the possibility to selectively control the growth of thin films on define regions over silicon substrates. Usually, the growth is only controlled in the normal direction to the surface, and time is the key parameter for the thickness control. Controlling the two other dimensions of a thin film, i.e., its lateral dimension in the plane, is usually obtained, thanks to the patterning top-down approach with masks and lithography.[1] Depending on the complexity of a device, patterning requires single as well as multiple exposure (multiple masks). For CMOS advanced nodes, it is assumed that lithography will dominate the wafer cost. Also, at the nanoscale dimension, misalignment errors may be critical for the viability of a device. Therefore, 3D structuration by a new bottom-up approach is needed. This must be time- and cost-effective. From all the proposed solution, one is more and more attractive and is called area selective deposition (ASD).[2,3] A good way to obtain such area selective deposition is to use atomic layer deposition (ALD), which is naturally sensitive to surface chemical states.[4–6]

Three main types of bottom-up growth with ALD have been proposed in the last years. The first method requires the activation of a specific region of the surface. As an example, Mackus *et al.* have proposed to combine electron beam induced deposition (EBID) and ALD.[7] EBID can be used to decompose any gas of molecules adsorbed on a substrate under an electron beam.[8–10] The second method is based on a surface passivation (or deactivation) from ALD growth.[11–14] One way to deactivate the surface is to use organic compounds such as self-assembled monolayers (SAMs)[15] or to deposit or implant thin hydrophobic groups like CF_x on a defined portion of the surface.[16,17] The aim is to chemically and locally bond a molecule, that may be viewed as a suppressor, directly on the surface in order to inhibit reactive sites and then prevent further reactions during ALD cycles. The SAM must be defect-free to limit severe selective issues, which may require extended SAM deposition times in liquid solutions, or self-correcting processes. Alternatively, the deposition time has been reduced using a vapor phase solution for SAM instead of usual liquid baths.[18,19] Another way to obtain ASD by ALD is to take benefits from the inherent selectivity observed with ALD processes.[20,21] This method relies on the inherent or modified nucleation delay between two different surfaces. Nucleation delay depends on many factors: the molecules used during ALD reaction,[22] the chemical nature of the surface (hydroxyl or hydrogenated bonds but also organic or inorganic surface…), the temperature of the substrate, etc. It has been shown that by choosing the adapted chemistry, substrate and temperature, it is possible to increase the nucleation delay of one surface against another which at the end induces a difference in the deposited thickness. Meanwhile, the maximum thickness obtained using this method is generally constrained below 10 nm. Finally, an alternative could be the mixing of two or three of the previous selective processes. As an example of this solution, Mameli *et al.* proposed an ABC cycle strategy for selective deposition with an inhibitor step inserted in each ALD cycle.[23]

In this work, an alternative approach discussed in a previous paper is proposed.[24] This atomic layer selective deposition is based on three requirements (see Fig. 1):

Note: This paper is part of the 2019 special collection on Atomic Layer Deposition (ALD).

a)Author to whom correspondence should be addressed: christophe.vallee@cea.fr

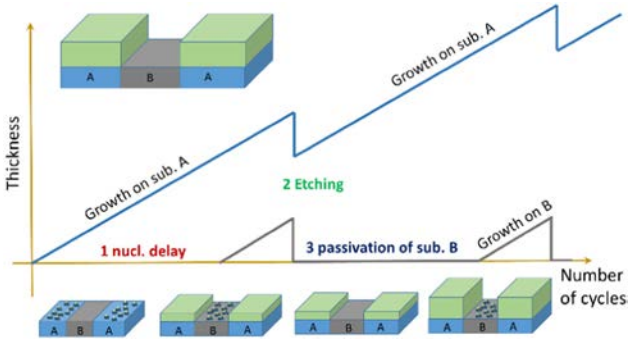

FIG. 1. Illustration of a selective deposition process based on the combination of PEALD and embedded plasma etching step.

(1) An inherent selectivity must exist between two regions with different surface chemistries in order to obtain a different nucleation time or delay. Hence, if selective deposition on surface A versus surface B is desired, the ALD growth must start first on surface A.
(2) A precise and selective etching process at the nanometer scale in order to remove the material that finally started to grow on the undesired region (surface B in our example). This step can be done using a plasma etching process.
(3) A chemical passivation step must be included in order to add a new nucleation delay for ALD on surface B.

All these three steps will define a "super ALD cycle." In our process, ALD is plasma assisted (PEALD). Therefore, a plasma etching was developed for the etching step. Different types of plasma etching modes may be used including RIE-like (reactive ion etching with both physical and chemical etching), "radicals only" (chemical—no ions), or quasi-Atomic Layer Etching. The choice of plasma etching mode depends on the geometry of the features where selectivity is required (i.e., horizontal versus vertical surfaces). Subsequently, the choice of the plasma etching will impact the isotropy or anisotropy. Most of the PEALD process chambers are designed in order to suppress the flow of ions onto the surface of the substrate. In this specific case, "radicals only" mode can be used, and it is the subject of the present work. Ideally, selectivity by ALD/Etching process could be obtained by combining ALD and atomic layer epitaxy (ALE) (or quasi-ALE). ALE is the reverse of ALD and is achieved using also sequential and self-limiting reactions.[25–28] From a definition point of view, ALD allows deposition at an atomic scale while ALE permits selective etching. Three examples of selective deposition are given in Fig. 2. For (a) and (b) patterned structures, the selective deposition must be obtained on the wall of the feature only. Then, an etching step must be added to remove any undesired deposition on top or bottom. Therefore, an anisotropic etching is needed. In the case of example (c), the selective deposition must be localized at the edge of the metal lines

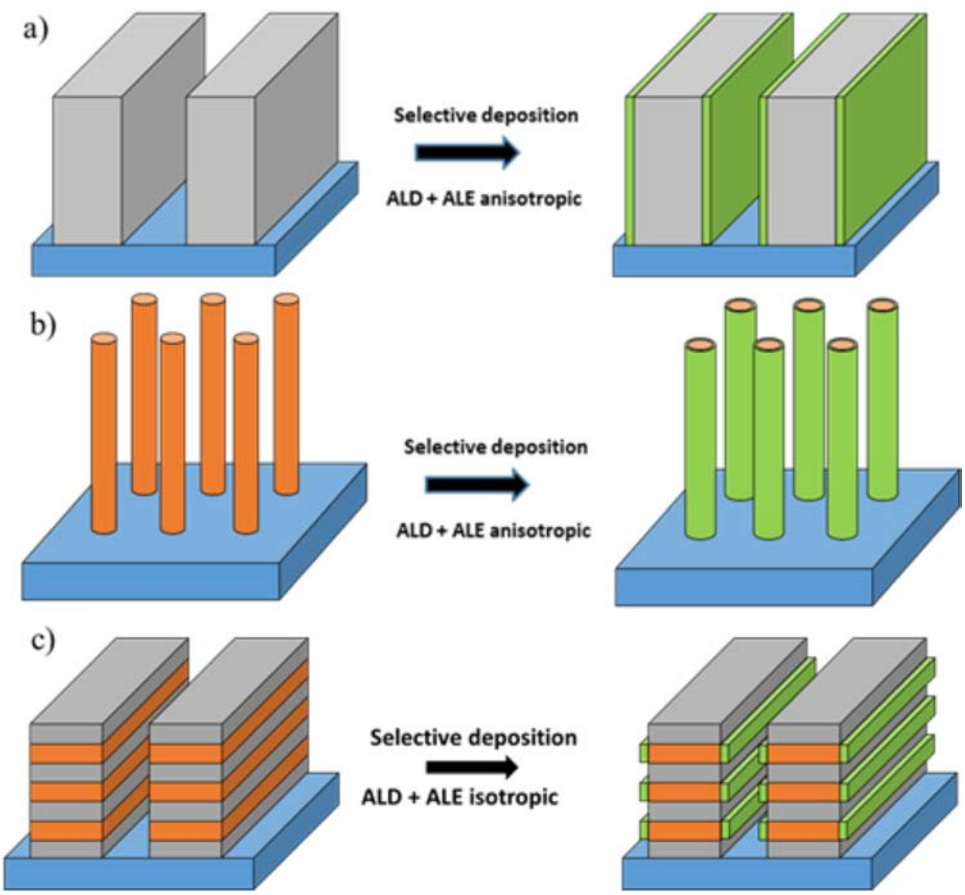

FIG. 2. Example of different selective processes on 3D patterned substrates.

only, then an isotropic etching is preferred in this case. In this paper, we will show results corresponding to this last example, i.e., the selective deposition at the edge of metal lines on 3D patterned substrates.

II. EXPERIMENT

A. PEALD reactor and TiO_2 deposition

The selective depositions are realized in a reaction chamber included a pulsed liquid injection system for precursors vaporization and plasma assistance on 200 and 300 mm wafers.[29] This versatile tool allows the deposition of oxides, metal nitrides in CVD, PECVD, ALD, or PEALD modes.[29–31] The deposition module consists of an evaporating furnace and a deposition chamber. The furnace is used for the flash vaporization of the liquid precursor. The liquid precursor is carried using He as a gas vector to the evaporating furnace where it is introduced, thanks to a liquid injector. The evaporated gas is then introduced in the deposition chamber through a showerhead with two separated paths: one for the precursor gas and one for the reactant gas. Tetrakis(DiEthylAmido) Titanium (TDEAT) liquid precursor is used in combination with an O_2 plasma for the PEALD deposition of TiO_2 oxide. For etching, NF_3 gas is used and is mixed to O_2 flow. The deposition chamber is a capacitively coupled plasma chamber with a distance of a few centimeters between the showerhead and the substrate holder. Two independently controlled generators can be used for powering the plasma at 13.56 MHz and/or 350 kHz. Both generators deliver the power at the showerhead, the substrate holder being grounded. For this paper, only the plasma in the 13.56 MHz mode has been used either for oxidation in PEALD ($Ar + O_2$ plasma) or etching ($Ar + O_2 + NF_3$) processes.

B. Characterization tools

Thickness, density, and roughness were measured by x-ray reflectivity (XRR), using a Jordan Valley JVX5200 for process development (deposition and etching) and using a Panalytical X'Per Pro tool for selective deposition tests (samples on holders). Chemical composition was measured by x-ray photoelectron spectroscopy (XPS) using a customized Thermo Scientific Theta 300, with Al-Kα, 400 μm and 100 eV beam. The parallel Angle Resolved capability of this tool (pAR-XPS) allowing to acquire eight angles (from 23.75° to 76.25°) without any sample tilt has been exploited for some acquisitions in order to extract depth resolved chemical information. An electron flood gun has been used for all acquisitions for better surface charge stability. A specific "Pfeiffer" carrier is used and allows the wafer transfer under vacuum from the deposition tool to the XPS characterization tool.[32] With this "Pfeiffer" carrier, *quasi-in situ* analyses (i.e., without air break) are carried out avoiding any surface unwanted air oxidation. Electrical characterizations in the DC mode were performed in air using a Keithley 2635a Source Meter unit, with the bottom electrode grounded. Roughness measurements were achieved using icon AFM in tapping mode, equipment from Brucker. The SEM pictures were acquired in S5000 tool from Hitachi at 30 kV.

III. RESULTS AND DISCUSSION

The three steps presented in Fig. 1 are decomposed and studied step by step. Then, all the individual steps will be grouped together at the end of this study in order to show the ALD selective process on a 3D pattern device as illustrated in Fig. 2(c).

A. Step 1: Inherent selectivity

The TDEAT precursor and O_2 reactive gas are pulsed separately into the deposition chamber. The TDEAT pulse duration is 4 s, while O_2 plasma pulse is 2 s at an RF power of 75 W. The O_2 gas is highly diluted, by a ratio of 1:10 in Ar gas (250 sccm of O_2 and 2500 sccm of Ar) in order to set the working pressure at 2 Torr.

The ALD window of TiO_2 PEALD process has been first established. Hence, 41 cycles on a standard Si substrate have been performed at seven different temperatures (110, 150, 200, 250, 300, 325, and 350 °C). The growth per cycle (GPC) as a function of deposition temperature is plotted in Fig. 3. Thicknesses were extracted from XRR measurements. The PEALD plateau (deposition limited by surface reactions) is well visible between 100 and 300 °C with an extracted GPC of 0.45 Å/cycle. This value is close to the typical value of 0.5 Å/cycle for TiO_2 by ALD.[33] Above 300 °C, the TiO_2 thickness increases strongly with the temperature, indicating the onset from ALD to CVD regime where the growth is mainly governed by the temperature. The deposition temperature is set on the plateau at 250 °C for the rest of the work. At this temperature, we are working in the ALD saturation regime. As an example, with the parameters used for this paper (4 s of TDEAT + 2 s of O_2 plasma), the GPC is 0.44 Å/cycles. With 10 s of precursor dose instead of 4 s, the

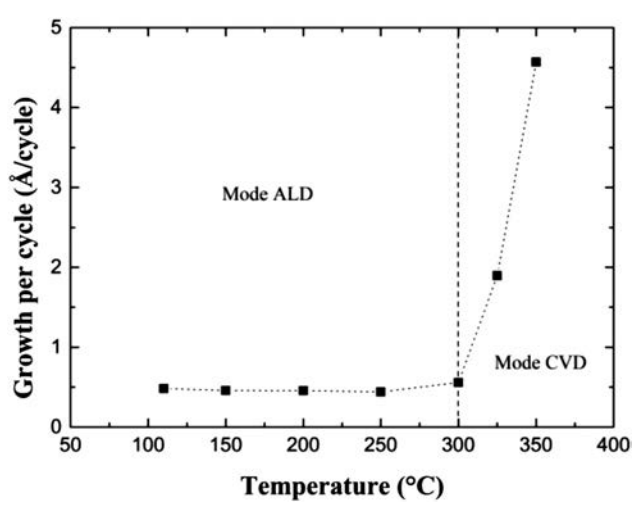

FIG. 3. PEALD windows of TiO_2 film with GPC measured by XRR vs substrate temperature.

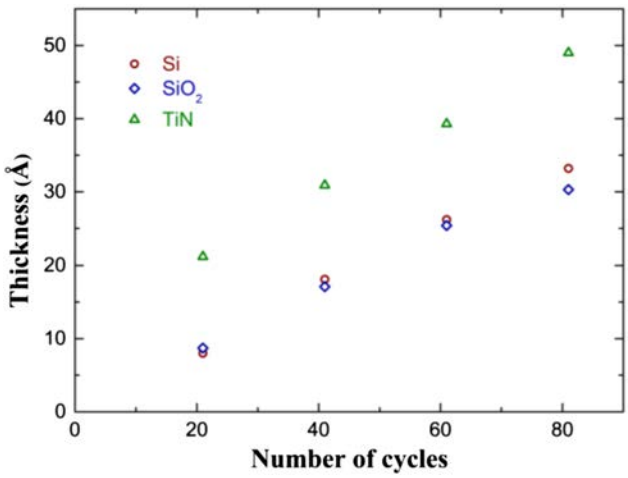

FIG. 4. TiO_2 film thickness measured by XRR vs the number of PEALD cycles on three different substrates: Si native, SiO_2, and TiN.

GPC is nearly the same, about 0.43 Å/cycles. With 4 s of O_2 plasma instead of 2 s, the GPC is 0.45 A/cycles.

Then, GPC and nucleation delay for PEALD of TiO_2 have been studied on different materials. For this purpose, three different substrates have been used: Si with native oxide (around 10 Å Si–O–H including C contamination from air), SiO_2 (well densified thermal oxide 100 nm), and TiN (stoichiometric 10 nm deposited on the Si substrate by physical vapor deposition). The growth per cycle and nucleation delay have been quantified using XRR measurements after 21, 41, 61, and 81 cycles. The corresponding data are shown in Fig. 4. The TiO_2 growth per cycle is quite identical on Si and SiO_2 substrates. The slope of the line for the TiN substrate is also similar, at around 0.45 Å/cycle, but the line is shifted with a constant value of approximately 1 nm.[34] Such a difference has already been observed for the deposition of Ta_2O_5.[24] Density and roughness of the TiO_2 layers deposited on each substrate have been determined using XRR measurements. The fitted densities of the titanium oxide materials are between 3.7 and 3.9 g/cm^3. These values are close to the 3.9 g/cm^3 theoretical value for anatase TiO_2.[35] Roughness values measured for all TiO_2 layers are close to 0.4 nm.

The TiO_2 growth rate at first cycles is clearly higher on TiN. To apprehend this effect, we achieved O_2 "plasma only" treatment on TiN. Therefore, TiN substrates were introduced in the deposition tool and exposed to O_2 plasma during 2 and 60 s. The other O_2 plasma parameters were kept constant (i.e., pressure, flux, power). After plasma exposure, the TiN samples were analyzed in a *quasi-in situ* mode by parallel angle resolved XPS, thanks to the vacuum carrier tool (i.e., no air break). A TiN substrate without any plasma exposure was also analyzed for reference. Figure 5 shows the Ti2*p* XPS core region at two "extreme" angles: Fig. 5(a) at 61.25° for near surface analysis and Fig. 5(b) at 23.75° to collect the maximum of signal intensity in sample depth. At 23.75°, the probe depth corresponds to three times the mean free path (λ) of the material studied.[36] The mean free path is about 1.5 nm for TiN material, so, at 23.75°, the beam probes around 4.5 nm.[37] The Ti2$p^{3/2}$ contributions are shown in this paper (and not Ti2$p^{1/2}$). Three different contributions are observed in Fig. 5: Ti–O bonds (Ti^{4+}) at 458.6 eV, Ti–O/N bonds (Ti^{3+}) at 456.9 eV, and Ti–N bonds at 455.4 eV.[38,39] At the TiN surface [Fig. 5(a)], Ti–N contribution disappears after 2 s O_2 plasma exposure. Also, the Ti–O/N contribution is strongly reduced. On the contrary, Ti–O contribution increases as soon as the TiN substrate is exposed to O_2 plasma. Deeper in the film [Fig. 5(b)], the same trends are observed. The difference between the two angles is evident for Ti–N contribution. Indeed, this contribution decreases at 23.75° but does not disappear since all the TiN is not converted into TiO_2. For the two angles, only the top surface TiN is strongly modified within seconds of plasma exposure. No significant evolution is observed for longer exposure times. Hence, a very fast modification of chemical bonds at the Ti–N surface is observed during the earliest seconds of O_2 plasma exposure with a shift from TiN to TiO_xN_y and TiO_2 bonds.

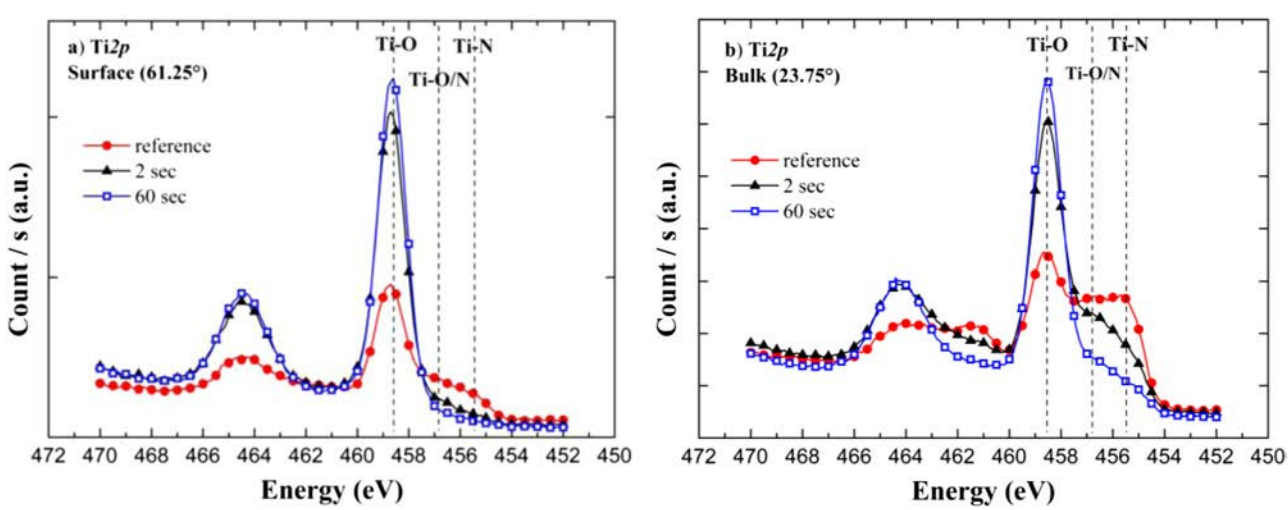

FIG. 5. Quasi-*in situ* XPS showing Ti2*p* peak of impact of O_2 plasma on the TiN substrate: (a) substrate surface at 61.25° and (b) substrate bulk at 23.75° (ref: C1s at 285 eV).

XPS data have been confirmed by XRR measurements (data not shown). The TiO_xN_y surface is mainly converted into TiO_2 during the first 2 s of O_2 plasma exposure. The TiO_2 thickness is around 1 nm which corresponds precisely to the difference of TiO_2 formation at TiO_2/TiN interface. This difference increases very slightly with plasma exposure time and confirms that the formation of 1 nm TiO_2 thickness appears during the first ALD cycles. One notices that on Si with native oxide, this effect is not visible since approximately 1 nm of native SiOx is already present on the top surface. This is even more obvious on 100 nm thick SiO_2. Consequently, we cannot evidence any nucleation delay between Si-based surface and TiN due to the O_2 plasma exposure.

B. Step 2: Etching of TiO_2 at the nanometer scale

As our goal is to add embedded plasma etching steps into TiO_2 deposition cycles, we studied in the same process chamber the effect of NF_3 etching on deposited PEALD TiO_2. For this purpose, an NF_3/O_2 based plasma at relative high pressure (in the Torr range) has been developed. In the deposition tool, the RF power is delivered to a metallic showerhead, and the substrate is grounded in order to limit ion bombardment. Then, by working in the Torr range, the ion sheath is mainly collisional, and the plasma etching mode is more or less like a "radical only" mode, without ion assistance, which is known to be quite isotropic.[26] NF_3 is used here because Fluorine based compounds are often used for Ti-based material etching in RIE or inductively coupled plasma mode since the boiling temperature of TiF_4 is very low at 248 °C.[40] This means that the etching step and the deposition can be performed at the same temperature and pressure, i.e., 250 °C and 2 Torr. In our previous paper, a very low Ta_2O_5 etching process was obtained using a very high dilution of NF_3 in O_2.[24] This process had the following parameters: $O_2/Ar/NF_3$ gases mixture of 250/2500/5 sccm and a very low RF power (75 W). We kept these parameters (dilution and plasma power) for this work. For the measurement of the etching rate as a function of time, first a TiO_2 thin film has been deposited by PEALD on a silicon planar wafer (300 mm) and not on patterned substrates. Then, this wafer has been cleaved in order to obtain six samples (TiO_2/Si) of the same size. Later, the samples have been put on a silicon holder and submitted to a different plasma etching time in order to obtain the etching rate as a function of time shown in Fig. 6. Thicknesses have been measured before and after etching by XRR. The etching rate is well controlled and very low, at about 1.9 Å/s.

Chemical bonding modifications induced by the plasma etching are investigated by *quasi-in situ* XPS. For that purpose, samples of TiO_2 layer with a thickness of 1.5 nm (41 cycles) were exposed to different plasma etching times. The evolution of Ti*2p* core region is presented in Fig. 7(a) as a function of the etching time every second. The Ti–O contribution is around 458.6 eV. As expected, the intensity of Ti–O decreases with the etching time. After 7 s of etching, Ti–O contribution fully disappears. All the TiO_2 layer thickness is etched. Figure 7(b) shows the F*1s* core region with two contributions: F–Ti around 684.5 eV and F–Si between 686.5 and 687 eV.[41,42] The F–Ti contribution increases first until 4 s and then decreases until it fully disappears at 7 s. In the meantime, an F–Si or OF–Si contribution appears at 4 s. This mechanism is also visible in Si*2p* presented in Fig. 7(c). Here, we extract two contributions, Si–O at 102.8 eV and Si–F/Si–OF at 103.8 eV.[43] The Si–O contribution shifts to higher energies during etching. The shift is explained by the presence of Si–F/Si–OF bonds. After 7 s, the TiO_2 is completely etched away on the Si substrate and a strong peak of Si–F bonds appears. Also, we observe the increase of Si^0 contribution at approximately 99 eV emerging from the Si substrate below TiO_2 which gradually increases while TiO_2 is etched. So, it is possible to draw a mechanism as follows: first, TiO_2 is converted to Ti–F which is volatile at 250 °C, then around 4 s, fluorine active species incoming from the plasma reaches the released substrate and forms Si–F. This process is quite gradual probably due to the evolution of TiO_2 roughness during etching. This will be discussed later in this paper.

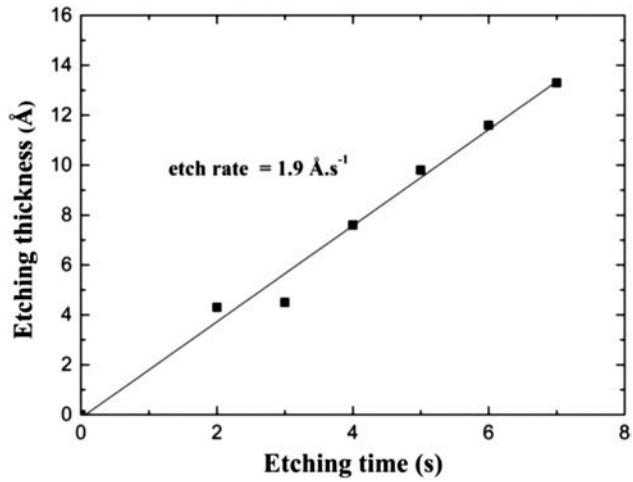

FIG. 6. TiO_2 etching rate using $O_2/Ar/NF_3$ gas mixture at 2 Torr, RF 75 W, and 250 °C. Data extracted from XRR measurement after well-adjusted fits.

C. Step 3: Passivation by fluorine plasma

As seen above, Si surface chemical states are strongly modified after etching with the presence of new Si–F/Si–OF bonds. So, in this part we study the impact of fluorine of the nucleation delay of TiO_2 on different substrates. For that purpose, a 5 s NF_3 "plasma only" was performed on Si, SiO_2, and TiN using the same previous conditions, i.e., a mixture of $NF_3/O_2/Ar$, 75 W at 2 Torr, followed by a standard PEALD-TiO_2 deposition in the same chamber and without air break. Here again, one each substrate, the growth per cycle has been calculated using XRR by evaluating the thickness of the TiO_2 film deposited in 21, 41, 61, and 81 cycles.

The thicknesses measured by XRR are reported in Fig. 8(a) for Si substrate and Fig. 8(b) for TiN. The figures show TiO_2 thicknesses versus cycles with and without NF_3 treatment for direct comparison. SiO_2 results are similar to

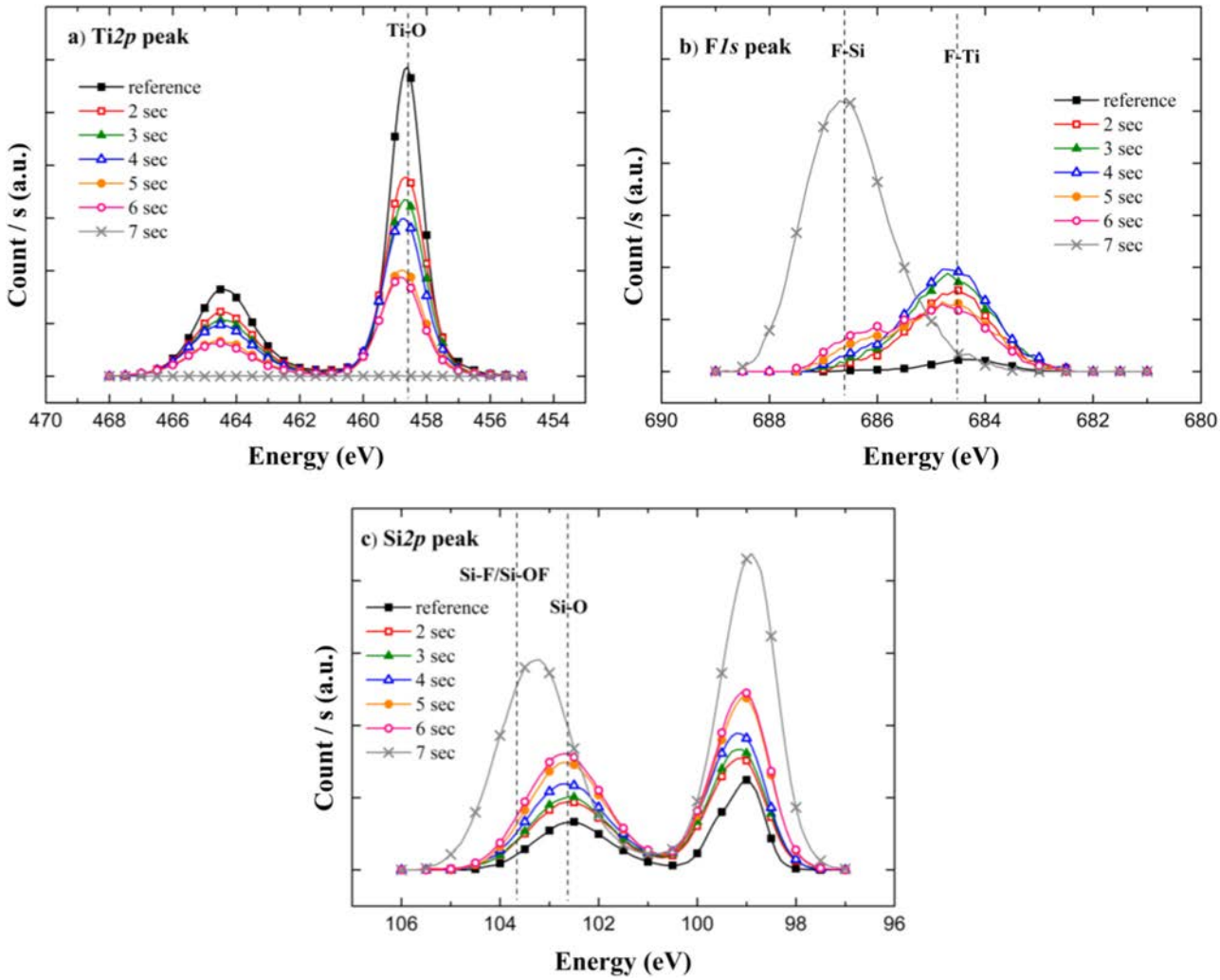

FIG. 7. Quasi-*in situ* XPS data showing the mechanisms of the etching process for TiO_2 layer (15 Å) by fluorine chemistry (a) Ti2*p* peak, (b) F1*s* peak, and (c) Si2*p* peak (ref: C1s at 285 eV).

the Si substrate (data not shown) as TiO_2 grows at the same rate on Si and SiO_2 substrates. On silicon, we clearly see a shift toward higher cycles due to the presence of nucleation delay. These incubation cycles can be estimated to roughly 10 cycles which results on a thickness difference of approximately 5 Å. On TiN, we nearly see no effects induced by the NF_3 pretreatment. Here again, around 1 nm is added to each point due to O_2 plasma impact on TiN (see step 1).

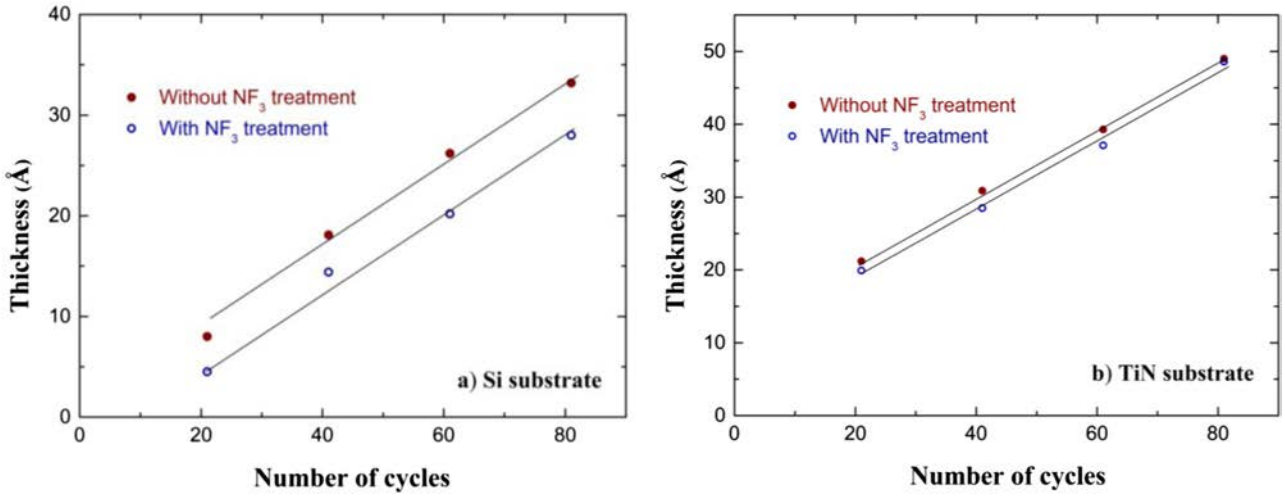

FIG. 8. TiO_2 film thickness measured by XRR vs number of PEALD cycles for untreated and NF_3 treated substrates; (a) on silicon surface, (b) on TiN metal.

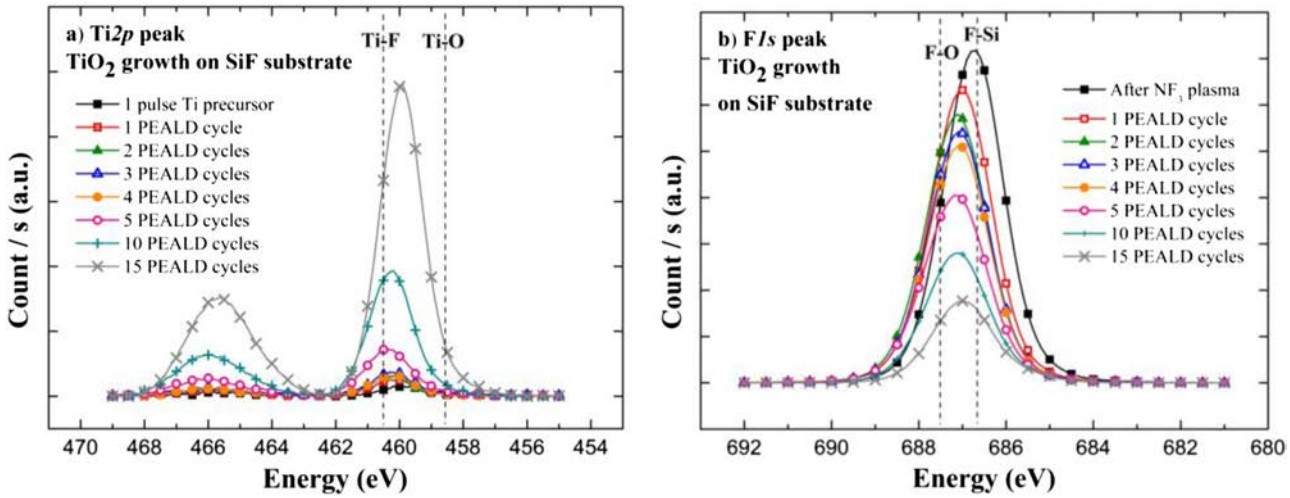

FIG. 9. *Quasi-in situ* XPS data of TiO_2 growing on the Si substrate pretreated by NF_3 plasma. (a) Ti2*p* core region and (b) F*1s* (ref: Si2*p* at 98.8 eV).

Figure 9 shows the *quasi-in situ* XPS analysis of Fig. 9(a) Ti2*p* and Fig. 9(b) F*1s* core regions for TiO_2 deposited on the 5 s NF_3 plasma Si–F terminated surface. First, only one pulse of the Ti precursor (half ALD cycle) is achieved (1 pulse duration is 4 s) to evaluate the chemisorption of the TDEAT on such fluorine surface. Then, 1, 2, 3, 4, 5, 10, and 15 full PEALD cycles were carried out. The Ti2*p* signal [Fig. 9(a)] is very weak for the first precursor exposure of the surface to TDEAT (half cycle), indicating that there are no reactions between the F terminated surface and the amine precursor. Stated differently, the surface is chemically inert regarding Ti core metal in TDEAT. This inert state is maintained during four PEALD full cycles which included O_2 plasma that completes each cycle. Even if O_2 plasma is exposed to the Si–F/Si–OF surface, the titanium precursor is nearly not grafted on the Si–F/Si–OF surface. After five PEALD cycles, the Ti2*p* peak intensity suddenly increases, suggesting that the Ti core metal begins to be grafted on the substrate inducing a first monolayer of TiO_2. F*1s* signal shows a complementary behavior as visible in Fig. 9(b). Indeed, the signal intensity is high from one to four PEALD cycles and becomes weaker after five PEALD cycles. Thus, Si–F/Si–OF bonds at the substrate ultimate surface inhibit TiO_2 growth during the first cycles; the growth is well limited for the first five PEALD cycles. After five cycles, the number of Si–F/Si–OF bonds and the density of F atoms at the surface decrease, enabling the TiO_2 growth.

To further understand how the amine precursor reacts at the surface, we achieved one half cycle of TDEAT on the untreated and F-treated (5 s of NF_3 plasma) Si substrate followed by *quasi-in situ* XPS analysis. The results are presented in Fig. 10. The Si–F bonds presence at the ultimate surface are visible on Si2*p* [Fig. 10(a)] while on the untreated Si substrate, only Si–O bonds are observed. Figure 10(b) shows that Ti precursor is immediately grafted on the Si substrate and not on Si–F/Si–OF. The energy position at 460 eV (instead of 459 eV for Ti–O) corresponds to Ti–O–Si bonding environment due to the electronegativity of silicon. Also, we observe a clear drop of Si^0 intensity in Si2*p* core region with Si–F treated surface while deposition of

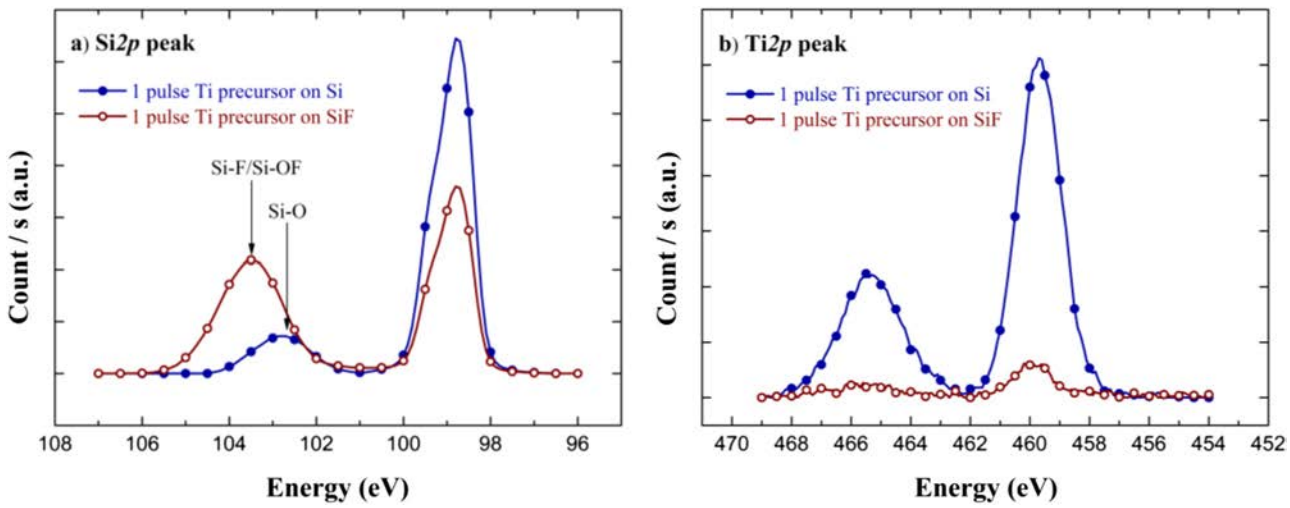

FIG. 10. Quasi-*in situ* XPS data for 1 pulse of TDEAT on Si and SiF substrates: (a) Si2*p* peak and (b) Ti2*p* peak (ref: Si2*p* at 98.8 eV).

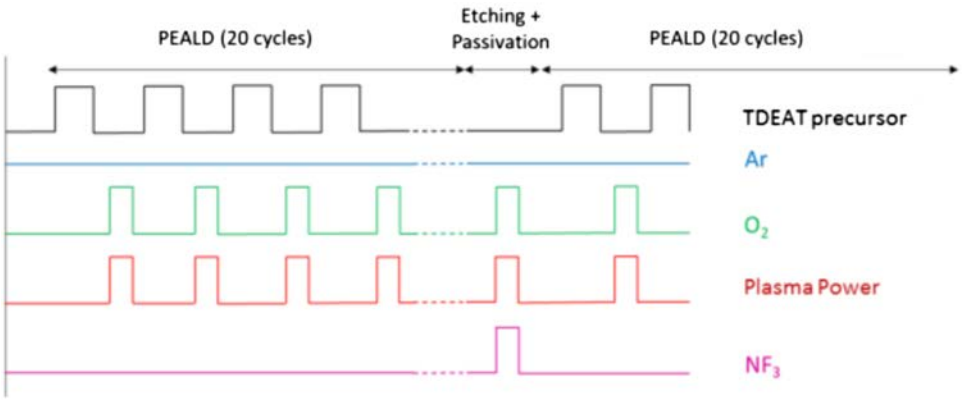

FIG. 11. Illustration of the selective deposition process. A super-cycle corresponds to 20 PEALD cycles + 3 s NF_3 plasma.

TiO_2 is effective on Si–O. One would expect the opposite behavior, but as the integrated surface below the curves in Fig. 10(a) is the same, this effect is more probably due to the screening effect of photoelectrons emerging from the Si substrate through Si–F layer (fluorine is highly electronegative). These facts confirm that Si–F/Si–OF bonds may limit the Ti core metal chemisorption during the first ALD cycles, and more interestingly even the impact of O_2 plasma that complete a PEALD cycle is not enough (in terms of plasma budget, i.e., time power) to release Si–F/Si–OF from the surface. In fact, in this particular case, at least five O_2 exposures are required to observe a significant TiO_2 growth at the surface.

D. Step 1 + step 2 + step 3 = Selective deposition of TiO_2

We join each individual step and build a "super-cycle" (PEALD + etching) process as summarized in Fig. 11. It includes 3 s of NF_3 etching step every 20 PEALD cycles. This "super-cycle" (PEALD + etching) can be repeated several times, depending on the desired oxide thickness.

Figure 12 shows the XRR spectra of Si, SiO_2, and TiN substrates after 12 super-cycles. As visible in this figure, the flat decrease of the acquisition intensities with no arches incoming from interferences between interfaces indicates that TiO_2 is not deposited on Si and SiO_2 substrates [Fig. 12(a)] while a thin film has been grown on the TiN substrate [Fig. 12(b)]. A modeling of the structure allows to extract the respective thickness, density, and roughness for the TiO_2 film deposited on TiN. The thickness of the TiO_2 film deposited with selective deposition process is 6.4 nm, the density is close to 3.9 g cm^{-3}, and the roughness is 0.9 nm after 12 super-cycles.

Standard XPS analyses (i.e., with air break) were also used to confirm the selective deposition on TiN substrate only. Figure 13 shows the O*1s* core region after processing on Si (a) and TiN (b) substrates after 12 super-cycles. For the Si substrate, the O*1s* spectrum can be fitted with two contributions: Si–O–Si/F bonds at 533 eV and O–C bonds at 531.7 eV.[44,45] The O–Ti contribution (expected around 530 eV) is not present, confirming that the growth of TiO_2 on Si and SiO_2 substrates is delayed. For the TiN substrate, there are also two contributions: O–C bonds at 531.7 eV and

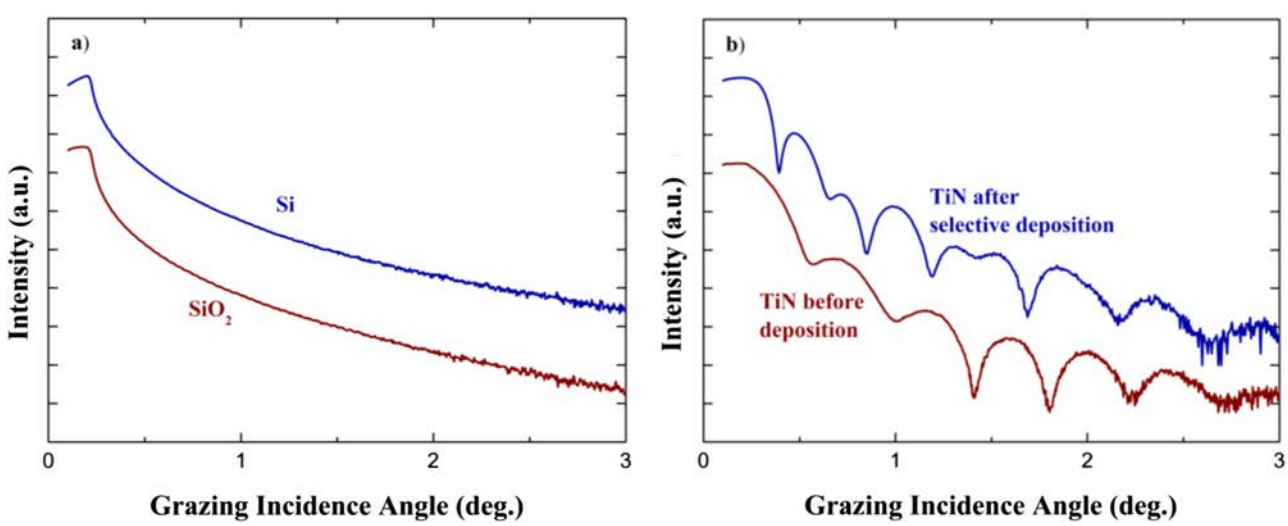

FIG. 12. (a) XRR graphs recorded after TiO_2 deposited on Si and SiO_2 substrates with the selective deposition process (12 super-cycles), (b) XRR graphs recorded before and after TiO_2 selectively deposited on the TiN substrate (12 super-cycles).

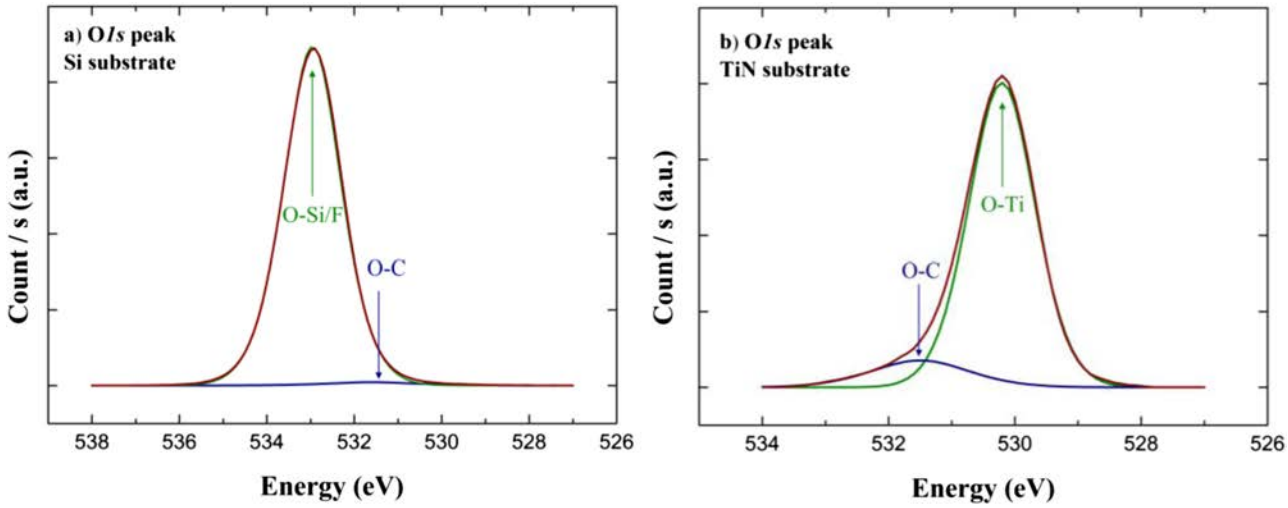

FIG. 13. XPS data showing O1s peak recorded after the selective deposition process (12 super-cycles) on the (a) Si substrate and (b) TiN substrate (ref: C1s at 285 eV).

O-Ti bonds at 530.2 eV.[46] The presence of Ti–O contribution attests the growth of TiO_2 on the TiN substrate. In this figure, C–O contribution is attributed to surface atmospheric contamination, here due to air break, and is useful to compare both graphs.

XRR measurements were then performed to obtain thickness and density versus the number of super-cycles. The data are presented in Table I. As expected, the oxide thickness increases with the number of super-cycles on the TiN substrate while TiO_2 density decreases from 4.0 to 3.7 g cm^{-3}. As an explanation to this reduction, we assume that the etching step adds fluorine in the oxide volume inducing a lower density. The Ti2*p* signal is not measurable from the XPS fit after 24 super-cycles deposition on Si and SiO_2 substrates. This means that less than 0.1% of Ti is present at the surface. One can notice that the TiO_2 thickness obtained on TiN after the selective deposition process slightly differs from the expected thickness by summing the GPC and etching rate previously and separately developed on planar substrates. As an example, after 12 super-cycles, the thickness of the selective TiO_2 film deposited is 6.4 nm while we were expected 5 nm from the sum of GPC and etching rate. Several effects can explain this difference:

- First, the plasma etching time used in a super-cycle is very short (3 s only). But the time takes by the automatic matchbox to move to the right tuning position is never the same and depends on its history. This signifies that there is a transient condition as the matchbox tune (typically 0.5–1 s here) that may induce a small shift in plasma properties (radicals, ions…) from one plasma step to another.
- Second, when adding an etching step to a deposition step we may have some cross contaminations due to byproducts or radicals sticking at the wall of the reactor that may modify the density of radicals or ions in the next step. As an example, NFx radicals from the plasma may react with an oxygen coated wall to form NOx and increase the density of F in the plasma. Hence, the etching rate for an etching step interposed in oxygen plasma may be different from a pure etching step without O radicals at the wall. For a better description, see, for example, the study from T. W. Kim and E. S. Aydil for the effect of chamber walls condition on silicon plasma etching.[47]

TABLE I. TiO_2 film thickness and density obtained from XRR measurements on Si, SiO_2, and TiN substrates after the selective deposition process.

Number of super-cycles	TiO_2 thickness on Si/SiO_2 (nm)	TiO_2 thickness on TiN (nm)	TiO_2 density (g cm^{-3})	Roughness XRR (nm)	Roughness AFM (nm)
6	0	4.3	4.0	0.8	0.5
12	0	6.4	3.9	0.9	1.0
24	0	11.6	3.7	1.5	2.5

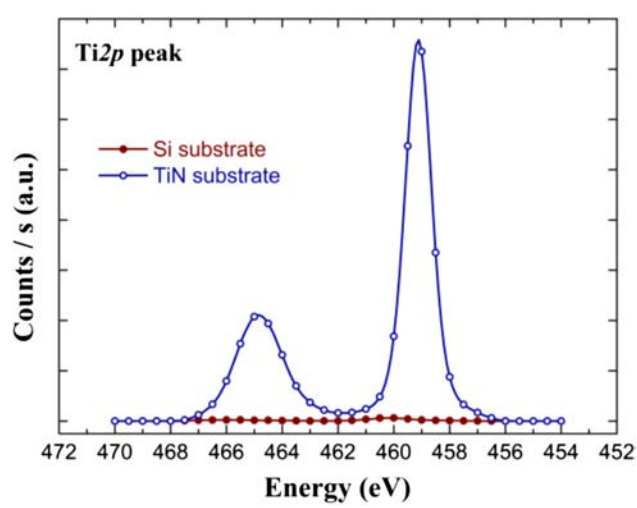

FIG. 14. XPS data showing Ti2*p* peak recorded after 24 super-cycles of selective deposition process on Si and TiN substrates (ref: C1s at 285 eV).

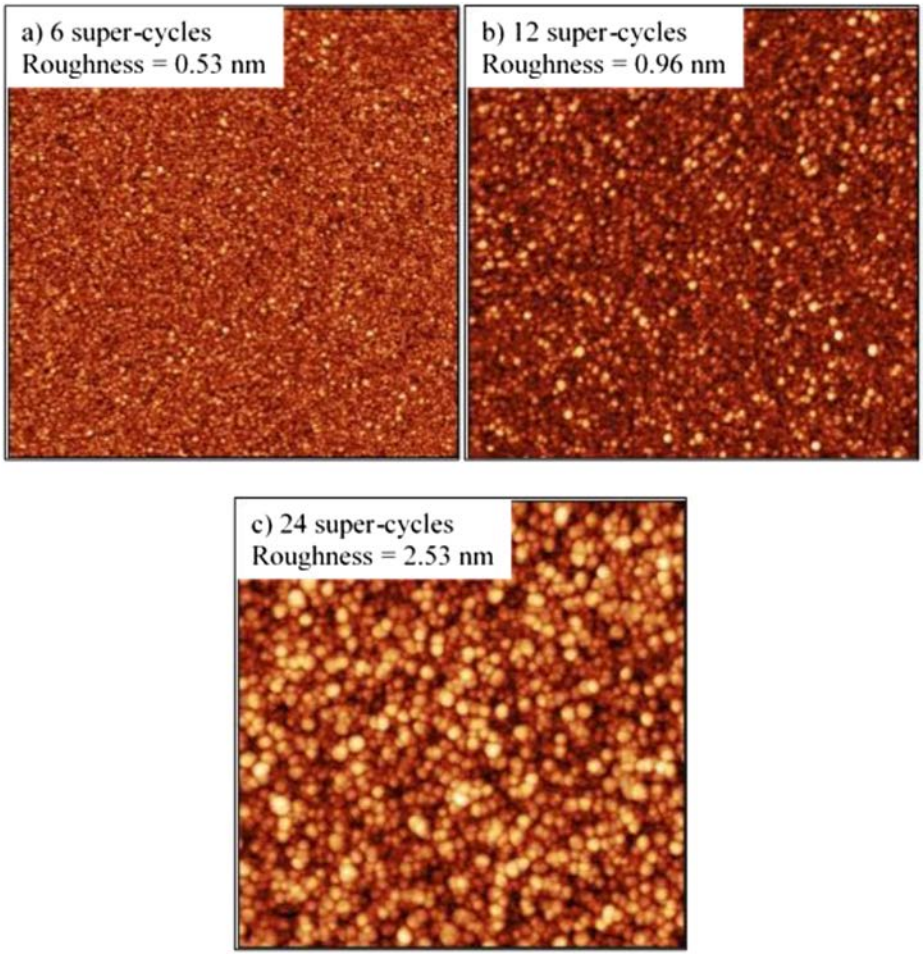

FIG. 15. AFM pictures of TiO_2 selective process recorded for (a) 6 super-cycles, (b) 12 super-cycles, and (c) 24 super-cycles.

To sum up, there exists a slight difference between the ASD "GPC" and the expected GCP (PEALD + etching) but this gives a very good starting point for the development of the ASD process.

The XRR results are confirmed by XPS measurements (Fig. 14). Ti2*p* peak is studied after 24 super-cycles on Si and TiN substrates. Nearly no Ti can be measured on the Si substrate (<0.1 at. %) which confirms the XRR results. In Table I, the roughness was extracted by XRR and using AFM for comparison. By modeling XRR data, a roughness variation is observed for the three TiO_2 samples. The roughness weakly increases with the selective thickness. AFM measurements allow to determine more precisely the roughness layers. The AFM pictures are shown in Fig. 15. Here, the roughness clearly increases with the number of super-cycles, from 0.53 nm (6 super-cycles) to 2.53 nm (24 super-cycles). As for the TiO_2 density, the fluorine step is surely accountable for the roughness increase. This effect is probably enhanced by the presence of crystalline grains, in particular, if TiO_2 is crystallized in the anatase structure, which is the case here at the deposition temperature (XRD data not shown). This is quite specific to TiO_2 since roughness increase has not been observed using Ta_2O_5 in our previous study, where in that case Ta_2O_5 is fully amorphous.[24]

E. Selective TiO_2 on 3D patterned substrate

After the optimization of the process on flat substrates, the effectiveness of this selective deposition method has been finally tested using a 3D architecture as shown

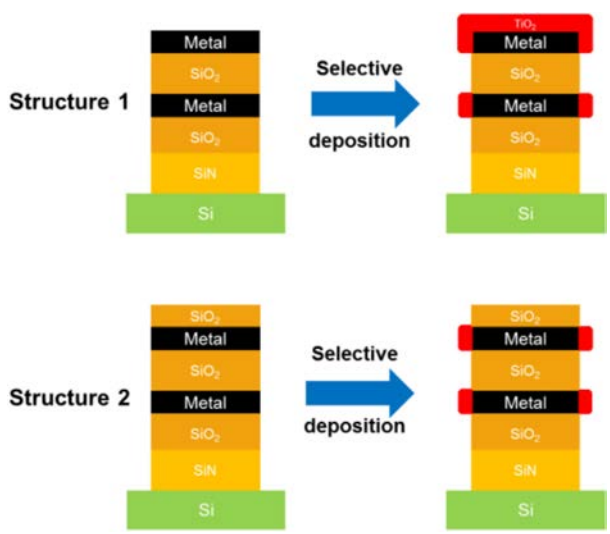

FIG. 16. Illustration of two 3D structures studied in this work before and after selective deposition.

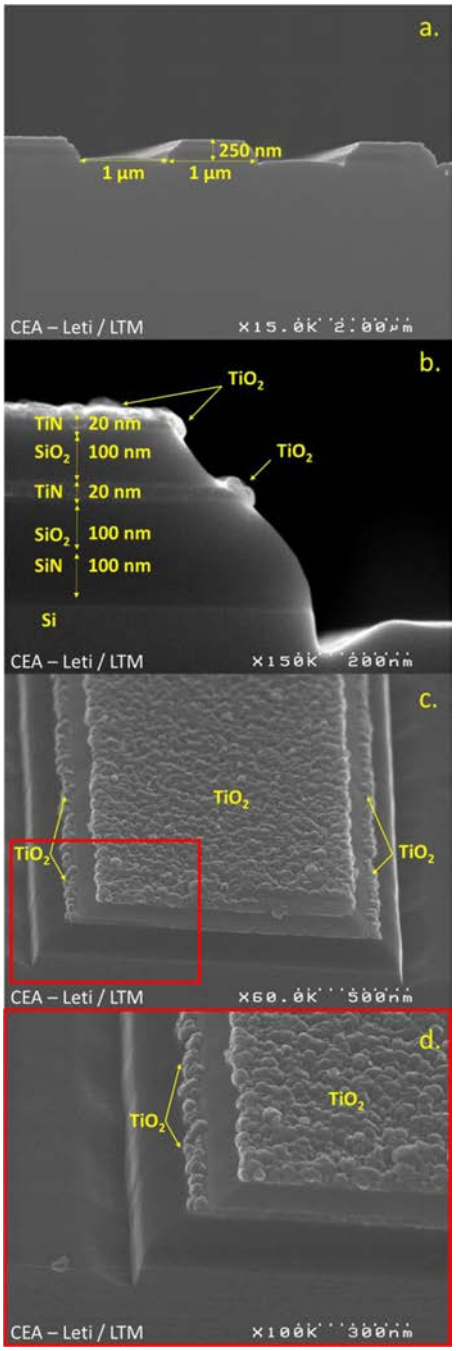

FIG. 17. SEM pictures (a) of the stack used, and on this stack after selective deposition of TiO_2 with (b) cross view, (c) top view, and (d) zoom on top view picture.

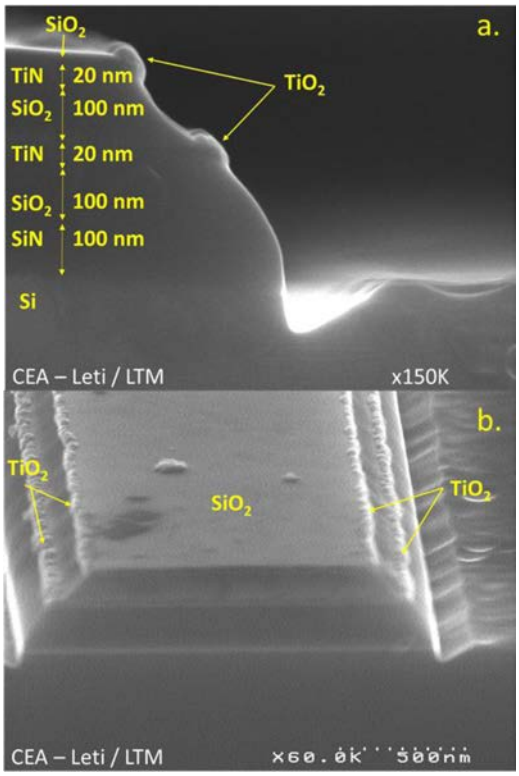

FIG. 18. SEM pictures of the 3D pattern device (structure 2) after the selective deposition of TiO_2 with (a) front view, (b) top view picture.

previously in Fig. 2(c). This 3D architecture is commonly used for the development of 3D Vertical memory devices. In this case, the objective is to deposit an oxide only at the edge of metal lines. In this work, two VRAM architectures are used as the case study as illustrated in Fig. 16; the final objective is to deposit TiO_2 only on the metallic surface, i.e., only at the edge of the two metal lines. The difference between structures 1 and 2 of Fig. 16 is the presence of an additional layer of SiO_2 on top of the pattern.

For the fabrication of the 3D device, SiN which acts as an etch stop layer is first deposited on the silicon wafer. After, the integration is based on stacking of multilayers, alternatively one SiO_2 layer then one metal layer of TiN. Finally, a photolithography step is achieved, followed by the etching of the structure to expose a portion of the TiN plan laterally on the structure wall. The TiN metal layer is surrounded by two dielectrics layers (SiO_2) and a TiN layer is deposited on top of the structure for structure 1 while two TiN metal layers are surrounded by SiO_2 layers in structure 2. The 3D column dimensions are typically 250 nm high and 1 μm wide [see Fig. 17(a)]. The plot is repeated every 1 μm. In these structures, the TiN layer thickness is fixed to 20 nm. Figures 17(b)–17(d) show the SEM pictures of the fabricated structure 1, after the selective deposition of TiO_2 using 24 super-cycles. It is observed that TiO_2 is successfully deposited only on the top of the TiN surface and at the edge of the TiN metal planes for the structure studied. Apparently, there is no deposition on the silicon-based surfaces, since no TiO_2 is observed by SEM on Si, SiO_2, or SiN surfaces. But we cannot exclude here the presence of very small growth clusters (nanometer dimension) that could not be detected by XPS or SEM images. TiO_2 deposited by the selective process is localized laterally on the 20 nm of TiN surfaces emerging on the sidewall of the structures, and not deposited on silicon-based surfaces on the sidewall. The TiO_2 thickness is around 20 nm (SEM measurement). On the SEM pictures, the TiO_2 is granular. Before, we have seen that etching has an impact on the roughness. So, this granularity is induced by the etching steps included in the selective process, probably due to the crystallization of TiO_2 in anatase.

SEM picture of the ASD of TiO_2 on structure 2 of Fig. 16 is shown in Fig. 18. Again, by using the ASD process developed (24 super-cycles), TiO_2 growth is strictly limited to the two edges of TiN metal lines. The developed isotropic chemical etching/passivation steps are sufficient to remove and add delay for the TiO_2 growth on any of the Si-based surfaces including Si, SiO_2, and even SiN.

IV. CONCLUSIONS

In this paper, by combining both TiO_2 growth, TiO_2 etching and NF_3 passivation, we have demonstrated the selective deposition of TiO_2 on TiN against Si/SiO_2 by including a plasma etching step into a PEALD standard process: NF_3 etching step is added every 20 cycles with a minor modification of the PEALD process parameters (same pressure and temperature) in order to selectively remove the TiO_2 layer from Si and SiO_2 only. Si–F bonds formed at the surface during this etching step help to increase the selective thickness by surface passivation before starting the PEALD growth of TiO_2 on Si or SiO_2 substrates.

This process has been applied successfully on the 3D structure using Vertical RAM architecture as the case study. Approximately, 20 nm of TiO_2 is deposited at the metal surface (TiN) and not on the silicon-based surfaces. Selective TiO_2 shows a certain degree of granularity due to the crystallization of this oxide in the anatase structure at low temperature. Fluorine tends to accentuate the roughness through preferential etching at grain boundaries. This effect seems specific to TiO_2 and it has not been observed with amorphous Ta_2O_5. This achievement is one of the first ASD process on 3D patterned surface at the nanometric scale. In the end, we think that combining PEALD and isotropic or anisotropic plasma etching (chemical etching or ALE) is a powerful technique for area selective deposition and can be a relevant process for new 3D architectures as may be needed for NAND, VRAM, or FinFet integration. Atomic layer selective deposition is a new bottom-up toolbox; used in conjunction with conventional lithography, it opens new areas in 3D patterning that would not be conceivable using standard top-down solutions.

[1]K. Galatsis *et al.*, Adv. Mater. **22**, 769 (2010).
[2]A. J. M. Mackus, A. A. Bol, and W. M. M. Kessels, Nanoscale **6**, 10941 (2014).
[3]R. Clark, K. Tapily, K.-H. Yu, T. Hakamata, S. Consiglio, D. O'Meara, C. Wajda, J. Smith, and G. Leusink, APL Mater. **6**, 058203 (2018).
[4]R. L. Puurunen, J. Appl. Phys. **97**, 121301 (2005).
[5]M. Leskelä and M. Ritala, Angew. Chem. Int. Ed. **42**, 5548 (2003).
[6]H. B. Profijt, S. E. Potts, M. C. M. van de Sanden, and W. M. M. Kessels, J. Vac. Sci. Technol. A **29**, 050801 (2011).
[7]A. J. M. Mackus, J. J. L. Mulders, M. C. M. van de Sanden, and W. M. M. Kessels, J. Appl. Phys. **107**, 116102 (2010).
[8]I. Utke, P. Hoffmann, and J. Melngailis, J. Vac. Sci. Technol. B **26**, 1197 (2008).
[9]W. F. van Dorp and C. W. Hagen, J. Appl. Phys. **104**, 081301 (2008).
[10]L. van Kouwen, A. Botman, and C. W. Hagen, Nano Lett. **9**, 2149 (2009).
[11]M. Yan, Y. Koide, J. R. Babcock, P. R. Markworth, J. A. Belot, T. J. Marks, and R. P. H. Chang, Appl. Phys. Lett. **79**, 1709 (2001).
[12]M. H. Park, Y. J. Jang, H. M. Sung-Suh, and M. M. Sung, Langmuir **20**, 2257 (2004).
[13]R. Chen, H. Kim, P. C. McIntyre, and S. F. Bent, Appl. Phys. Lett. **84**, 4017 (2004).
[14]R. H. A. Ras, E. Sahramo, J. Malm, J. Raula, and M. Karppinen, J. Am. Chem. Soc. **130**, 11252 (2008).
[15]H.-B.-R. Lee and S. F. Bent, "Nanopatterning by area-selective atomic layer deposition," in *Atomic Layer Deposition of Nanostructured Materials*, edited by N. Pinna and M. Knez (Wiley, Weinheim, Germany, 2012).
[16]A. Hader, P. Deminskyi, T. M. Khan, H. Eren, and N. Biyikli, J. Phys. Chem. C **120**, 26393 (2016).
[17]W. H. Kim *et al.*, ACS Nano **10**, 4451 (2016).
[18]S. J. F. Herregods, L. Lecordier, S. Vyas, B. T. Chan, T. Delande, I. Hetel, Z. Tokei, H. Struyf, and S. Armini, *Proceeding of the Conference: Joint EuroCVD 21 – Baltic ALD 15*, Linköping, Sweden (2017).
[19]E. Farm, M. Vehkamaki, M. Ritala, and M. Leskela, Semicond. Sci. Technol. **27**, 074004 (2012).
[20]A. Sinha, D. W. Hess, and C. L. Henderson, J. Vac. Sci. Technol. B **24**, 2523 (2006).
[21]S. E. Atanasov, B. Kalanyan, and G. N. Parsons, J. Vac. Sci. Technol. A **34**, 01A148 (2016).
[22]K. J. Hughes and J. R. Engstrom, J. Vac. Sci. Technol. A **30**, 01A102 (2012).
[23]A. Mameli, M. J. M. Merkx, B. Karasulu, F. Roozeboom, W. M. M. Kessels, and A. J. M. Mackus, ACS Nano **11**, 9303 (2017).
[24]R. Vallat, R. Gassilloud, B. Eychenne, and C. Vallée, J. Vac. Sci. Technol. A **35**, 01B104 (2017).
[25]K. J. Kanarik *et al.*, J. Vac. Sci. Technol. A **33**, 020802 (2015).
[26]V. M. Donnelly and A. Kornblit, J. Vac. Sci. Technol. A **31**, 050825 (2013).
[27]K. Nojiri, Dry Etching Technology for Semiconductors (Springer, Tokyo, Japan, 2016); M. Yu *et al.*, *Sci. Rep.* **6**, 21020 (2016).
[28]S. M. George and Y. Lee, ACS Nano **10**, 4889 (2016).
[29]F. Piallat, C. Vallée, R. Gassilloud, P. Michallon, B. Pelissier, and P. Caubet, J. Phys. D Appl. Phys. **47**, 185201 (2014).
[30]F. Piallat and J. Vitiello, J. Vac. Sci. Technol. B **34**, 021202 (2016).
[31]M. Aoukar, P. D. Szkutnik, D. Jourde, B. Pelissier, P. Michallon, P. Noé, and C. Vallée, J. Phys. D Appl. Phys. **48**, 265203 (2015).
[32]B. Pelissier, H. Kambar, E. Godot, E. Veran, V. Loup, and O. Joubert, Microelectron. Eng. **85**, 151 (2008).
[33]J.-P. Niemelä, G. Marin, and M. Karppinen, Semicond. Sci. Technol. **32**, 093005 (2017).
[34]R. Katamreddy *et al.*, ECS Trans. **16**, 113 (2008).
[35]A. L. Linsebigler, G. Lu, and J. T. Yates, Jr., Chem. Rev. **95**, 735 (1995).
[36]T. Kajiyama, N. Morotomi, S. Hiraoka, and A. Takahara, Chem. Lett. **16**, 1737 (1987).
[37]G. G. Fuentes, E. Elizalde, F. Yubero, and J. M. Sanz, Surf. Interface Anal. **33**, 230 (2002).
[38]A. C. Bronneberg, C. Höhn, and R. van de Krol, J. Phys. Chem. C **121**, 5531 (2017).
[39]X. Shi, L. Xu, T. B. Le, G. Zhou, C. Zheng, K. Tsuru, and K. Ishikawa, Mater. Sci. Eng. C **59**, 542 (2016).
[40]S. K. Kwon, K. H. Kwon, B. W. Kim, J. M. Park, S. W. Yoo, K. S. Park, and Y. Kyu, ETRI J. **24**, 211 (2002).
[41]G. Liu, C. Sun, H. G. Yang, S. C. Smith, L. Wang, G. Q. Lu, and H. Cheng, Chem. Commun. **46**, 755 (2010).
[42]T. J. Chuang, J. Appl. Phys. **51**, 2614 (1980).
[43]H. Ogawa, T. Arai, M. Yanagisawa, T. Ichiki, and Y. Horiike, J. Appl. Phys. **41**, 5349 (2002).
[44]S. S. Chao, Y. Takagi, G. Lucovsky, P. Pai, R. C. Custer, J. E. Tyler, and J. E. Keem, Appl. Surf. Sci. **26**, 575 (1986).
[45]B. Folkesson and P. Sundberg, Spectrosc. Lett. **20**, 193 (1987).
[46]M. Takagi-Kawai, M. Soma, T. Onishi, and K. Tamaru, Can. J. Chem. **58**, 2132 (1980).
[47]T. W. Kim and E. S. Aydil, J. Electrochem. Soc. **150**, G418 (2003).